International Journal of Heat and Mass Transfer 194 (2022) 122988

Contents lists available at ScienceDirect

International Journal of Heat and Mass Transfer

journal homepage: www.elsevier.com/locate/hmt

Graphene coated 3C-SiC with improved irradiation resistance and enhanced heat conduction property after collision cascade

Xiaona Huang, Jiang Guo, Yanan Yue*

Key Laboratory of Hydraulic Machinery Transients (MOE), School of Power and Mechanical Engineering, Wuhan University, Wuhan, Hubei 430072, China

ARTICLE INFO

Article history:
Received 21 January 2022
Revised 16 April 2022
Accepted 29 April 2022
Available online 7 May 2022

Keywords:
Thermal transport
Interface
Irradiation resistance
Graphene/SiC composite

ABSTRACT

Graphene/SiC nanocomposites are promising materials with excellent irradiation resistance. In this study, the structure of 3C-SiC coated with graphene layers is proposed to improve SiC's irradiation resistance. The atomistic mechanisms behind the irradiation resistance and irradiation's effect on the thermal conductance of the composite are investigated through molecular dynamics simulations. Results show that the graphene layers effectively enhanced the irradiation resistance of SiC in the composite with increased threshold displacement energy when irradiated with a carbon primary knock-on atom (PKA). Influence factors, i.e., graphene layer number, incident angle of the PKA, and temperature, of irradiation resistance are also studied by collision cascade simulations. In addition, the heat conduction of the composite is enhanced after the irradiation with the 1.5 keV carbon PKA. The resistance dominates the thermal transport at the graphene layers near the interface instead of the interface. The largest temperature drop occurs between the interface and the penultimate graphene layer, consistent with the significant mismatch of their vibrational density of states. After irradiation with the 1.5 keV carbon PKA, the thermal conductance of the graphene/SiC composites increases, and the interface thermal resistance decreases due to the formed bonds between the graphene layers. Overall, this work provides a fundamental understanding of the irradiation resistance and the thermal properties of the graphene/SiC composite.

1. Introduction

Silicon carbide (SiC) possesses outstanding properties of good temperature stability, corrosion resistance, creep resistance, high-temperature conductivity, and irradiation resistance [1,2]. Thus, it is a candidate material for developing equipment or electronic devices used in environments with high irradiation levels, high temperatures, and chemically active surroundings in the nuclear industry, aerospace technology, and medical applications [3]. SiC is a covalent compound with many allotropes (e.g., 3C-SiC, β-SiC, 4H-SiC, and 6H-SiC). 3C-SiC with zinc blende structure has been mostly used in nuclear reactors. Under irradiation environments, primary knock-on atoms (PKAs) are induced from irradiation. Then they trigger collision cascades resulting in defect formation and degrading the mechanical and thermal properties of SiC. Thus, improving irradiation resistance is essential to enhance the performance of SiC.

Graphene, a two-dimensional nanomaterial, exhibits extraordinary intrinsic properties of ultra-high mechanical strength, thermal and chemical stability, and good thermal conductivity, rendering graphene a promising material used for many applications [4]. Many researchers verified the performance of graphene in irradiation resistance. Ochedowski et al. investigated the deterioration of transistors based on MoS_2 and graphene due to the irradiation with swift heavy ions and found that the MoS_2 transistor was destroyed while the graphene-based one still worked [5]. Graphene layers can reduce the thermal spike intensity in copper-graphene nanocomposite because the hard C–C bonds of graphene hinder the penetration of irradiation atoms with their energy dissipated along the graphene planes [6,7]. The graphene-aluminum composite shows remarkable irradiation resistance under high-energy helium irradiation due to the excellent sink strength of graphene for irradiation-induced point defects [8]. Kumar et al. [9] conducted the radiation experiments of graphene residing on the growth substrate by Au ions with the energy of 150 MeV and fluences of $1 \times 10^{11} \sim 1 \times 10^{14}$ ions/cm^2, and found that graphene retains a significant fraction of crystallinity after irradiated. Navarro et al. [10–12] conducted several experiments to study the performance of graphene as a coating to protect tungsten against ion sputtering and found that graphene has successfully provided some protection to tungsten against surface damage at high helium flu-

* Corresponding author.
E-mail address: yyue@whu.edu.cn (Y. Yue).

https://doi.org/10.1016/j.ijheatmasstransfer.2022.122988
0017-9310/

ences. The properties of graphene mentioned above suggest that graphene layers on the surface of SiC can act as the protective layer from irradiation, which has been rarely investigated.

In addition, high heat-conducting property is preferred during the service period of nuclear reactors (e.g., light water reactor, future fusion reactor, and high-temperature gas-cooled reactor) [13]. Good thermal conductivity enables graphene to be filled in thermal management materials. In particular, graphene has a strong anisotropy in thermal conductivity, ultra-high in plane and relatively low cross plane. Thus, coating graphene layers on the SiC surface introduces additional resistance, i.e., the resistance of graphene layers and the interface thermal resistance between graphene layers and SiC. The interface thermal resistance due to the phonon scattering is detrimental to the thermal conductivity of composites [14,15]. The interfacial thermal conductance between graphene and substrate has been studied via experiments and simulations [16]. For example, the interfacial thermal conductance between graphene and SiC was influenced by the atom bonds and substrate crystallinity, which is higher in graphene/a-SiC than in graphene/c-SiC from molecular dynamics (MD) simulations [17]. Zhang et al. measured the thermal diffusivity and interfacial thermal conductance of substrate supported graphene sample via Raman spectroscopy method [18,19]. It is essential to investigate the heat transfer performance of composites during the irradiation process. The heat-conducting property change of graphene/SiC composites after irradiation and its mechanisms have not been fully understood.

The detailed irradiation process and the consequent structure changes are challenging to detect experimentally due to the short temporal scale and small spatial scale. MD simulation with the atomic resolution and femtosecond time scale is a powerful tool that complements experimental characterization, which has been widely used in irradiation and thermal conductivity studies [20–23]. In reality, graphene coating has many layers with complex microstructure, including graphene flacks and interfaces, and the sample can be exposed to long-term radiation. However, due to the limitation of MD simulation, our work only focuses on the initial stage of radiation damage of SiC coated with several layers of graphene initiated by a PKA. In this work, 3C-SiC coated with graphene layers serves as an irradiation-resistant material. The irradiation resistance and the thermal conduction before and after irradiation are investigated via MD simulations. The composite with more graphene layers shows a higher threshold displacement energy (E_d) of SiC. In the collision cascade simulations, lower peak and stable vacancies are produced in SiC coated with more graphene layers; no clear relationship exists between the incident angle and irradiation resistance; the peak vacancy number increases with the rise of temperature. Besides, the interface thermal resistance between graphene layers and SiC decreases after irradiation. Our study paves the way for graphene application in irradiation resistance materials.

2. Methodology

2.1. Interatomic potentials

The Tersoff potential in combination with the Ziegler-Biesack-Littmark universal screening function (ZBL) (Tersoff-ZBL potential) [24,25] is used to describe 3C-SiC and the interactions between the 3C-SiC and graphene sheets. The Tersoff potential developed by P. Erhart et al. reproduces the elastic and thermal properties of the 3C-SiC well and describes graphite effectively [24]. The ZBL potential, a repulsive interaction description, describes the collision process with short-range distances [25,26]. The parameters (A_F and r_C) for the fermi-like function to connect the Tersoff and ZBL potentials are shown in Table 1 [25]. A_F controls the sharpness of their transition, and r_C is the cutoff for the ZBL potential. The graphene layers are described by the adaptive intermolecular reactive empirical bond order (AIREBO) potential [27].

Table 1
The parameters (A_F and r_C) for the fermi-like function to connect the Tersoff and ZBL potentials.

Bond	A_F ($Å^{-1}$)	r_C (Å)
C-C	15	0.82
C-Si	30	0.46
Si-Si	30	0.55

2.2. Model construction

Researches show that graphene can be fabricated through epitaxial growth on SiC without catalyst, and there is covalent bonding between graphene and SiC [28–30]. This work focuses on the structure of epitaxial graphene growth on a 3C-SiC substrate. Small composite models of SiC coated by graphene layers are built to estimate E_d. The SiC supercell is built by replicating the unit cell by 10 × 10 × 10 with X, Y, and Z oriented [100], [010], and [001] directions, respectively. It consists of 8000 atoms with the dimensions of 43.80 $Å$ × 43.80 $Å$ × 43.80 Å, which is large enough for E_d calculation [31]. The graphene layers are built through replicating the orthogonal graphene cell by 10 × 17 × 1 with X, Y, and Z oriented [$\bar{1}$10], [$\bar{1}\bar{1}$0], and [001] directions, respectively, and the distance between layers is 3.4 Å. The graphene layers are stretched by 2.8% and 4.7% along the X and Y axes to match the SiC supercell's size. SiC and graphene are found to form a strong covalent bond with a distance of 1.65 ± 0.05 Å, which can be well described with the Tersoff–ZBL potential [32,33]. Thus, the graphene layers are placed 1.7 Å above the SiC supercell. An 11.6 Å vacuum layer is set along the Z axis to build the model for E_d calculations. The composite models with 2, 4, and 8 layers of graphene are built to investigate the influence of graphene layer thickness on irradiation resistance. Similarly, large composite models with a 23.2 Å vacuum layer are built by replicating SiC and graphene layers by 20 × 20 × 20 and 20 × 34 × 1, respectively, to conduct collision cascade simulations (see Fig. 1).

2.3. E_d calculation and collision cascade simulations

After energy minimization, the small composite models are relaxed under the canonical (NVT) ensemble at 300 K for 50 ps. Then, a carbon atom is inserted as a PKA at 4 Å above the upper surface center of the model along the Z axis. The PKA is pushed along the given direction with the specific energy varying on the 1.0 eV grid. After 20 ps evolution of the system under the microcanonical (NVE) ensemble, the final configuration is checked for any stability defect. According to previous research, displacement behavior is probabilistic at some kinetic energies [31]. Thus, 16 independent simulations are conducted at each PKA energy using the system configuration randomly selected from the relaxation stage. E_d is the lowest energy that generates a stable defect in at least one of the 16 simulations.

Cascades are simulated using the large composite models irradiated with a 1.5 keV PKA. After energy minimization and 100 ps relaxation under the NVT ensemble, the PKA irradiates into the system along the given direction from 4 Å above the top layer graphene. The system evolves 20 ps under the NVE ensemble to investigate system damage due to the PKA bombardment. An automatically adapted time step is applied during PKA bombardment and in E_d calculation, in which the time step is re-computed every step to avoid atoms moving further than 0.017 Å in one time step.

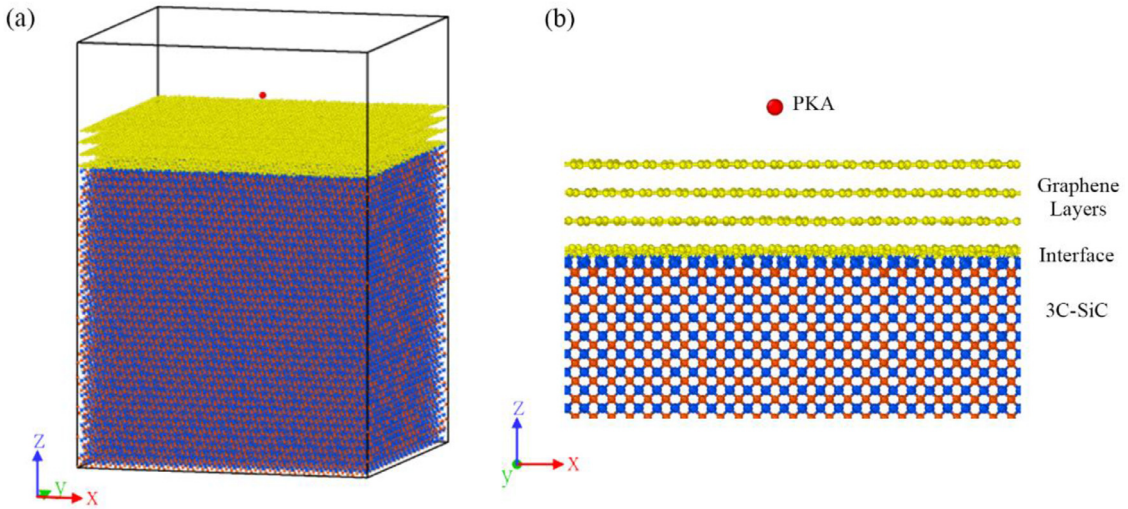

Fig. 1. (a) Schematic diagram of the large composite system with four graphene layers. (b) Composite interface aligned with the (010) plane. The PKA, carbon atoms in graphene layers, silicon, and carbon atoms in SiC are marked in red, yellow, blue, and pink, respectively.

Five independent cascade simulations with different initial velocity distributions are conducted to avoid contingency results and obtain the average damage. The incident angle is 7° with respect to the Z direction to reduce channeling effects in E_d calculation and collision cascade simulations, with velocity components in the X and Y directions remaining equal. Besides, the collision cascade simulations with different incident angles of 27, 47, and 67° are also conducted to investigate the incident angle's influence on irradiation responses.

2.4. Thermal conductance calculation

The thermal conductance of the composite part between the heat source and heat sink is calculated via the non-equilibrium MD method (NEMD), which includes all graphene layers (except the heat source) and 3 nm thickness SiC as shown in Fig. 2. The atoms in the 57 Å lower part of SiC along the Z axis are fixed to reduce computation. The mobile part is initially relaxed sequentially under the NVT and NVE ensembles for 100 ps at 300 K. Then, the first graphene layer serves as the heat source. The 3 Å atoms above the fixed SiC serve as the cold source (see Fig. 2). The temperatures of the heat and cold sources are maintained at 400 K and 200 K, respectively, using the Langevin thermostat [34] with a damping parameter of 0.1 ps. The NEMD simulations are performed for 1.0 ns under the NVE ensemble to build a steady-state temperature gradient. The thermal conductance per unit area $G(L)$ at length L can be written as [35]

$$G(L) = \frac{J}{\Delta T} \tag{1}$$

where ΔT is the temperature difference between the heat source and the cold source. J is the nonequilibrium steady-state heat flux, which can be calculated from $dQ/(dtS)$, where Q is the thermal energy across a cross-sectional area S perpendicular to the transport direction, and t is time. Q is equal to the cumulative energy added/subtracted to the heat source/sink, which can be obtained from MD simulation software directly.

The vibrational density of states (VDOS) provides phonons vibration mode strength with frequency. The system is relaxed under the NVE ensemble with the time step of 0.5 fs for 15 ps to calculate VDOS from the trajectories extracted every 5 fs. VDOS is obtained from the fast Fourier transformation [36] of the velocity autocorrelation function (VACF) [13,37].

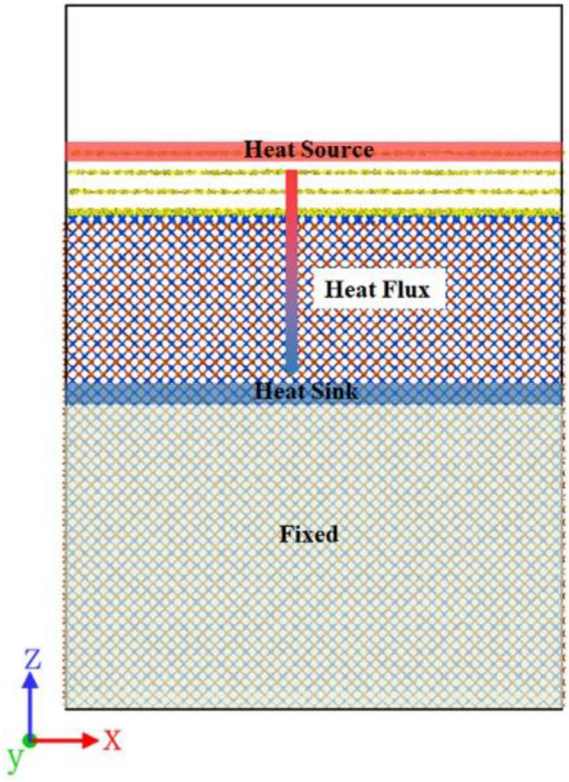

Fig. 2. Schematic of the NEMD simulation setup. The carbon atoms in graphene layers, silicon, and carbon atoms in SiC are marked in yellow, blue, and pink, respectively.

$$\mathrm{VDOS}(w) = \frac{1}{\sqrt{2\pi}} \int_0^{\tau} e^{iwt} \langle v(t)v(0)\rangle dt \tag{2}$$

where w is the phonon frequency; v is the velocity of atoms; t is the correlation time of VACF.

All the simulations in this work are conducted using the large-scale atomic/molecular massively parallel simulator (LAMMPS) software [38]. The conjugate gradient algorithm is applied during the energy minimization, and the velocity Verlet algorithm is used

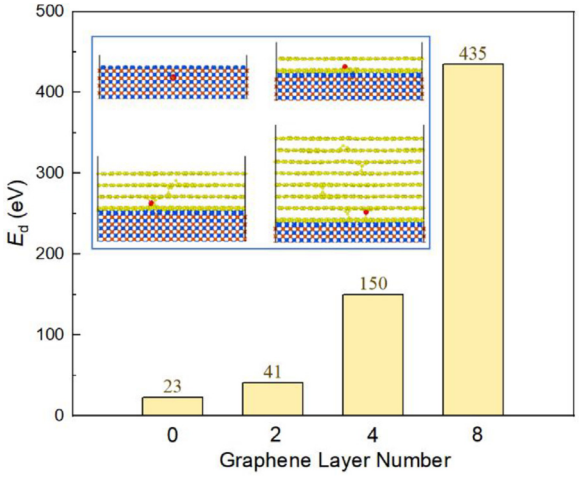

Fig. 3. E_d of small composite systems with different graphene layers. The insets are the local structures of the final configurations in E_d calculations. The PKA, carbon atoms in graphene layers, silicon, and carbon atoms in SiC are marked in red, yellow, blue, and pink, respectively.

during dynamic simulations with the time step of 1.0 fs unless otherwise specified. The periodic boundary conditions are used in the X and Y directions, and fixed boundary conditions are used in the Z direction. The temperature is controlled by Nose-Hoover thermostatting with the damping parameter of 0.1 ps unless otherwise specified. Defects are identified using the Wingner-Seitz analysis implemented in the open visualization tool (OVITO) [39].

3. Results and discussion

3.1. Threshold displacement energy

E_d is an essential parameter in understanding the irradiation behavior of nuclear materials. The E_ds of C atom in SiC without or with graphene layers are calculated and illustrated in Fig. 3. In our simulations, the E_d for bare SiC is estimated to be 23 eV, consistent with other research works of 13.5–40 eV [31,40–43]. The E_d increases rapidly with the graphene layer thickness with the value of 41, 150, and 435 eV for 2, 4, and 8 layers of graphene, which is 1.78, 6.52, and 18.91 times compared to that of the bare SiC, respectively. The results indicate that when coated with graphene layers, higher energy is needed to produce stable defects in SiC, resulting in enhanced irradiation resistance. The snapshots at the end of the simulations (see the insets in Fig. 3) show that the PKA irradiates into SiC when no graphene is coated. However, the PKA is blocked between the graphene layers in the composite systems, which means that the graphene layers can effectively dissipate PKA's energy. The defects in graphene layers are induced by the collision cascade, during which permanent structural damages occur with sp3 carbon atoms and C–C bonds between graphene layers formed.

3.2. Irradiation resistance from collision cascade simulations

The PKA with higher energy than E_d initiates collision cascades. The vacancy-interstitial pairs increase rapidly due to the collision at the ballistic phase. The displacement spike is reached when the recombination rate of vacancy-interstitial pairs equals their production rate. Then, the defect number decreases due to the recombination of vacancy-interstitial pairs and the decrease of high-energy atom number at the quenching phase. Cascade simulations with the PKA energy of 1.5 keV are conducted to investigate the irradiation resistance. Fig. 4 compares cascade simulation results of the bare SiC and SiC coated with different graphene layers. The vacancy number and PKA kinetic energy evolutions are similar in process and overall shape for the collision cascades of different systems. The vacancy number rises rapidly at the beginning of the collision and reaches a peak at around 0.13 ps. At this stage, the PKA loses most of its kinetic energy. Then, the high energy of the dislocated atoms dissipates, and more recombination occurs during quenching. The quenching time of SiC coated with different layers of graphene is similar. The number of Frenkel pairs produced per cascade can be estimated by the formula [44] $N = 0.8E_{PKA}/2E_d$, where E_{PKA} is the PKA kinetic energy. With the PKA energy of 1.5 keV and E_d of 23 eV, the peak vacancy number is estimated at 26, which is constant with our results of 19.6 ± 6.6, showing the validity of our simulations. The peak vacancy number is 19.6, 16.0, 15.0, and 5.0, and the stable vacancy number is 10.6, 9.5, 8.6, and 2.5 for the bare SiC and SiC coated with 2, 4, and 8 layers of graphene (denoted as SiC2G, SiC4G, and SiC8G). The results indicate that more graphene layers lead to lower peak and stable vacancy numbers. The PKA kinetic energy evolutions (see Fig. 4(b)) indicate that PKA in the system with more graphene layers is more likely to collide with other atoms and sharply lose energy by hard-core elastic scattering [22].

Graphene/SiC composite differ in atom arrangement for different directions resulting in various irradiation resistance. Fig. 5 compares the cascade simulation results of SiC4G with different PKA incident angles. The vacancy number peaks at around 0.12 ps at the incident angle of 7, 27, and 47°, and peaks at about 0.22 ps at 67°. Then, vacancy-interstitial pairs recombination and remain stable after about 1.0 ps. Meanwhile, the PKA energy rapidly decreases at the ballistic phase with approximately 0.5%, 18.2%, 0.3%, and 30.8% of the initial energy is remained at the end of the phase for the incident angle of 7, 27, 47, and 67°, respectively. The peak vacancy number is 15.0, 8.4, 14.4, and 6.0, and the stable vacancy number is 8.8, 7.0, 7.4, and 4.8 at the incident angle of 7, 27, 47, and 67°, respectively. The PKA kinetic energy evolutions are similar at the four incident angles. More vacancies occur at the incident angles of 7 and 47 compared to those at 27 and 67 The results indicate no clear relationship between the incident angle and irradiation resistance. We infer that the hard-core elastic scattering leads to more high-energy atoms at the incident angle of 7 and 47°, producing more vacancies.

Temperature has a significant influence on irradiation damage [22]. Fig. 6 compares the cascade simulation results of SiC4G at different temperatures. Similar to the results mentioned above, the defect number remains stable after 1.0 ps, and most PKA energy dissipates. The peak vacancy number possesses an increasing trend with the rise of temperature, which is 15.0, 15.6, 19.2, and 22.6 at 300 K, 600 K, 900 K, and 1200 K, respectively. The results may be due to the enhanced thermal motion at higher temperatures, making the atoms easier to dislocate. However, the survival vacancy number is 8.8, 7.4, 15.0, and 10.6 at 300 K, 600 K, 900 K, and 1200 K, respectively. Thus, temperature has little effect on the survival vacancy number in our simulation range of 300–1200 K, which agrees with the results from the cascade simulations for 3C-SiC with various PKA energies in the temperature range of 300–1800 K [25]. In detail, compared to 600 K, the collision cascade at 300 K produces a similar number of vacancies due to the stronger hard-core elastic scattering, although the temperature is lower.

3.3. Irradiation influence on thermal transport properties

Thermal conductance and interfacial thermal resistance are essential for the performance of composite materials. The thermal properties of the unirradiated and three irradiated configurations (final configurations after three independent cascade simulations) of SiC4G and SiC8G are studied through NEMD calculations. The

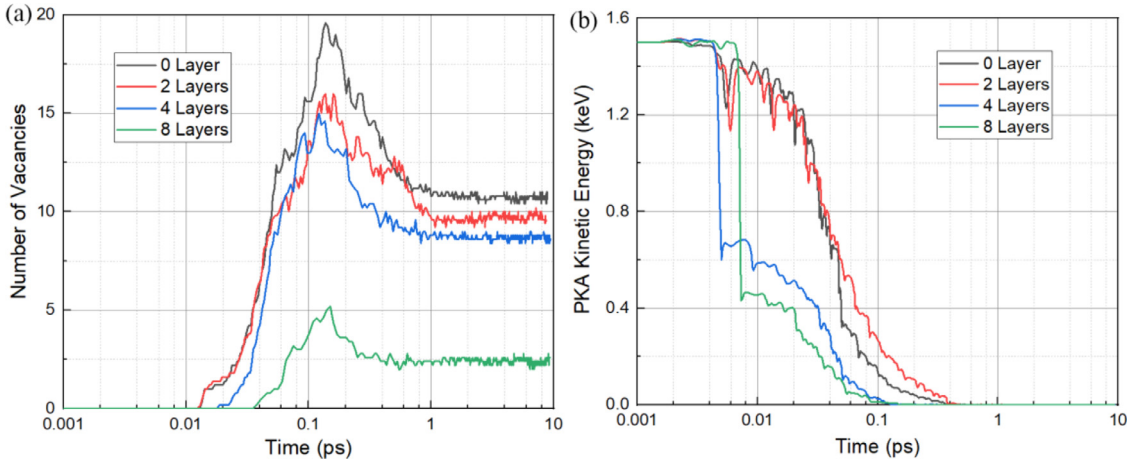

Fig. 4. (a) Vacancy number evolution and (b) PKA kinetic energy evolution during collision cascade initiated by a 1.5 keV carbon PKA in systems with different graphene layers.

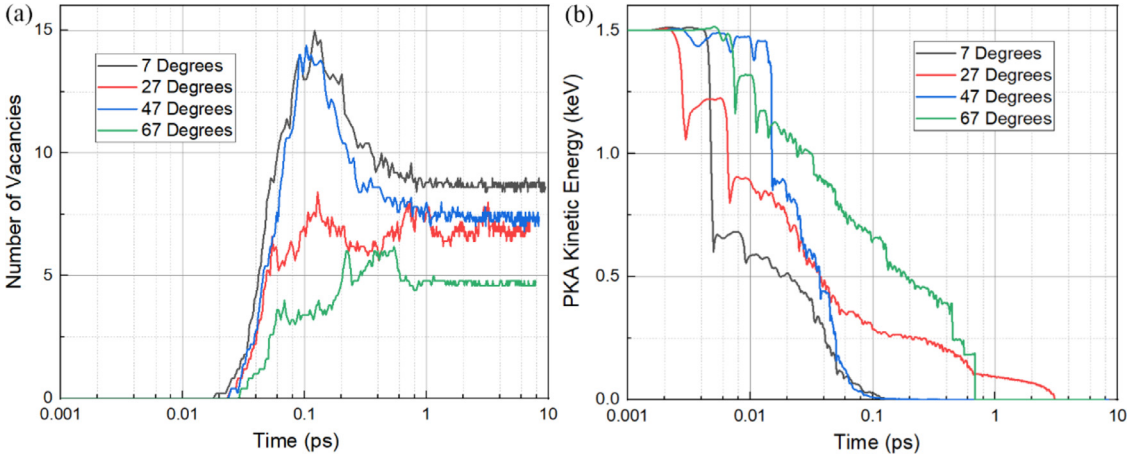

Fig. 5. (a) Vacancy number evolution and (b) PKA kinetic energy evolution during collision cascade initiated by a 1.5 keV carbon PKA with different incident angles in SiC4G.

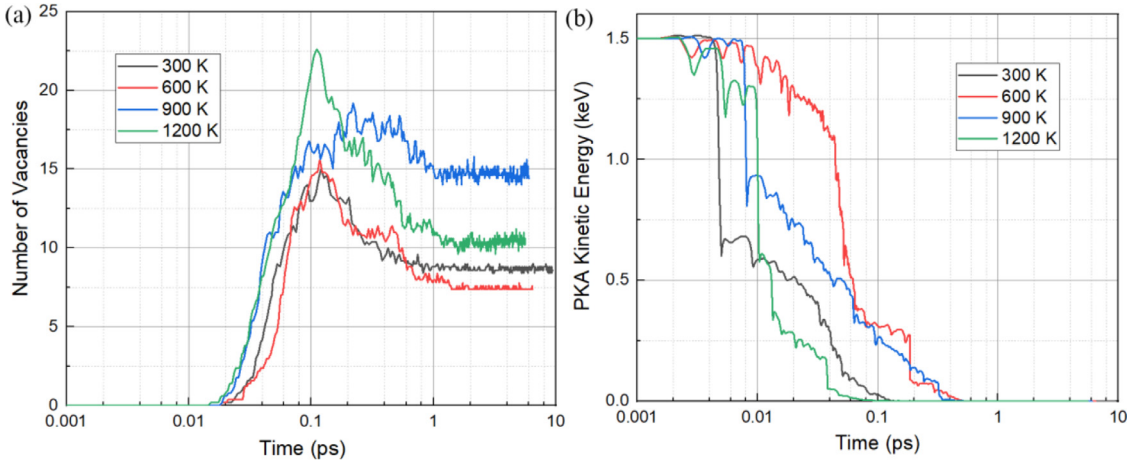

Fig. 6. (a) Vacancy number evolution and (b) PKA kinetic energy evolution during collision cascade initiated by a 1.5 keV carbon PKA at different temperatures in SiC4G.

effect of SiC thickness on the cumulative energy change and temperature profiles in the NEMD simulations for SiC4G is explored first, as shown in Fig. S1. Due to the different thicknesses of SiC (3 nm and 8.4 nm), the cumulative energy change and temperature profile in SiC have slight changes. However, SiC thickness has little effect on the temperature of graphene layers and the interface SiC. Besides, the interface thermal resistance is 1.32×10^{-8} $m^2 \cdot K/W$ and 1.35×10^{-8} $m^2 \cdot K/W$ when SiC thickness is 8.4 nm and 3 nm, respectively. Thus, SiC thickness has little effect on the interface thermal resistance. The composite with 3 nm thickness SiC is used to conduct NEMD simulations in this study.

In SiC4G, the heat flux increases after irradiation, which indicates that the heat transfer of the composite is enhanced (see Fig. 7). For the temperature profiles, the temperature slop in graphene

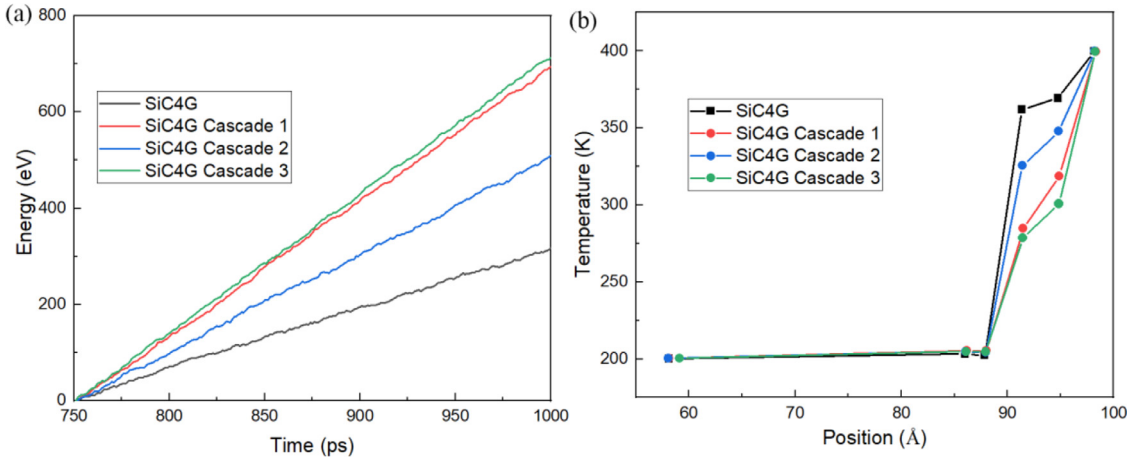

Fig. 7. (a) Cumulative energy change of the heat source/sink and (b) temperature profiles in the NEMD simulations for SiC4G.

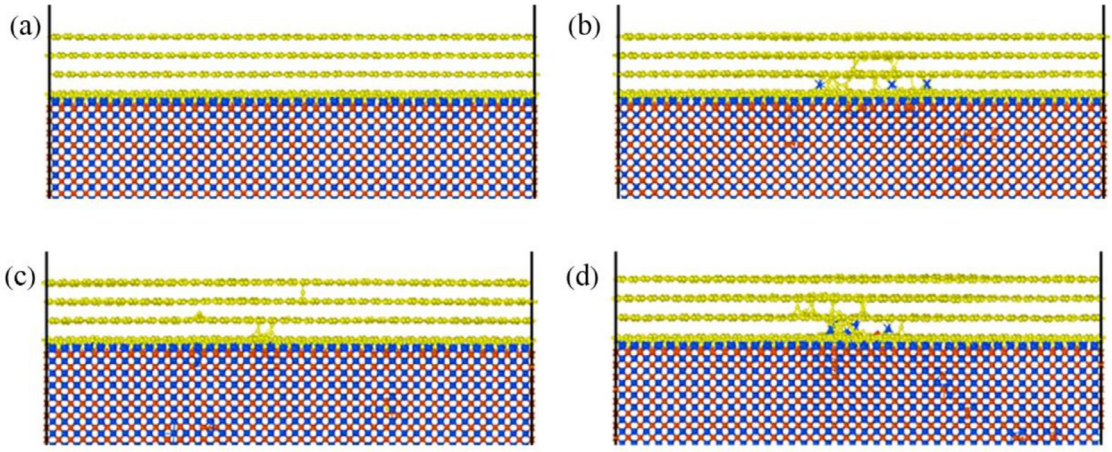

Fig. 8. Interface structures of SiC4G: (a) before irradiation, after (b) cascade 1, (c) cascade 2, and (d) cascade 3. The carbon atoms in graphene layers, silicon, and carbon atoms in SiC are marked in yellow, blue, and pink, respectively.

layers is much higher than that in SiC due to the much higher thermal conductivity of SiC. Due to the interface thermal resistance, an obvious temperature drop occurs near the interfacial region. In detail, the most significant temperature drop locates between the 3rd and 4th layer graphene instead of the interface. The reason is that the 4th layer of graphene is strongly bonded with SiC, which agrees with the reported results that the resistance at the near-interface region dominates the overall interfacial thermal transport while not the interface for strongly coupled interfaces [45]. The temperatures of the inner graphene layers decrease after irradiation compared to those before irradiation, which is consistent with the energy change. Meanwhile, the interface temperature difference decreases, showing enhanced heat transfer near the interface region.

The interface structures show that irradiation induces the atom dislocation in graphene layers after cascade simulations (see Fig. 8). Several defect configurations are produced in the graphite layers. For example, point defects and hole defects occur with more or less six atoms in the carbon rings, and defects are induced due to the introduction of the out-of-plane carbon atoms, even silicon atoms (see Fig. 8(b) and (d)). The heat flux is higher, and the temperatures of the inner graphene layers are lower after cascades 1 and 3 than cascade 2 due to more bonds formed between graphene layers. The thermal conductance between the heat source and the cold source is calculated and summarized in Table 2. The interface thermal resistance between SiC and graphene layers is shown in Table 3. The interface temperature drop is denoted by the temperature difference between the penultimate layer of graphene and the interface SiC. Consistent with the heat flux and temperature profile, the thermal conductance increases by 126.2%, 63.1%, and 132.3% after cascades 1, 2, and 3, respectively. Meanwhile, the interface thermal resistance decreases by 77.9%, 53.4%, and 79.9% after cascades 1, 2, and 3 compared to the unirradiated one, respectively. Besides, when irradiated with a 1.5 keV silicon PKA, the temperature profile is similar to that after irradiation with a carbon PKA (see Fig. S2). The thermal conductance and interface thermal resistance are 2.55×10^{7} W/(m^2·K) and 2.24×10^{-8} m^2·K/W, respectively. Thus, the heat conduction property is also enhanced after irradiating with a silicon PKA.

Fig. 9 shows the cumulative energy changes and temperature profiles in SiC8G. Similar to the results of SiC4G, the heat flux is higher, and the temperature of the inner graphene layers is lower after irradiation than the unirradiated one. The largest temperature drop also occurs between the interface graphene layer and the 7th graphene layer. Irradiation produces many defects in graphene layers with bonds and carbon atoms between atom layers (see Fig. 10). The results show that although single layer graphene may be defective, the covered SiC is not exposed (see Fig. S3). In most cases, the dislocated carbon atoms are confined between graphene layers by sp2 or sp3 bonding, resulting in the amorphous carbon structure formation. The amorphous carbon structure can reinforce graphene interlayer strength and continue to resist radiation. Be-

Table 2
Thermal conductance (G, in $\times$ 10^7 W/(m^2·K)) of non-irradiated and irradiated SiC4G and SiC8G.

System	SiC4G				SiC8G			
	Before irradiation	Cascade 1	Cascade 2	Cascade 3	Before irradiation	Cascade 1	Cascade 2	Cascade 3
G	1.30	2.94	2.12	3.02	1.37	2.27	2.52	2.40

Table 3
Interface thermal resistance (R, in $\times$ 10^{-8} m^2·K/W) of non-irradiated and irradiated SiC4G and SiC8G.

System	SiC4G				SiC8G			
	Before irradiation	Cascade 1	Cascade 2	Cascade 3	Before irradiation	Cascade 1	Cascade 2	Cascade 3
R	6.11	1.35	2.85	1.23	5.79	2.34	1.81	2.30

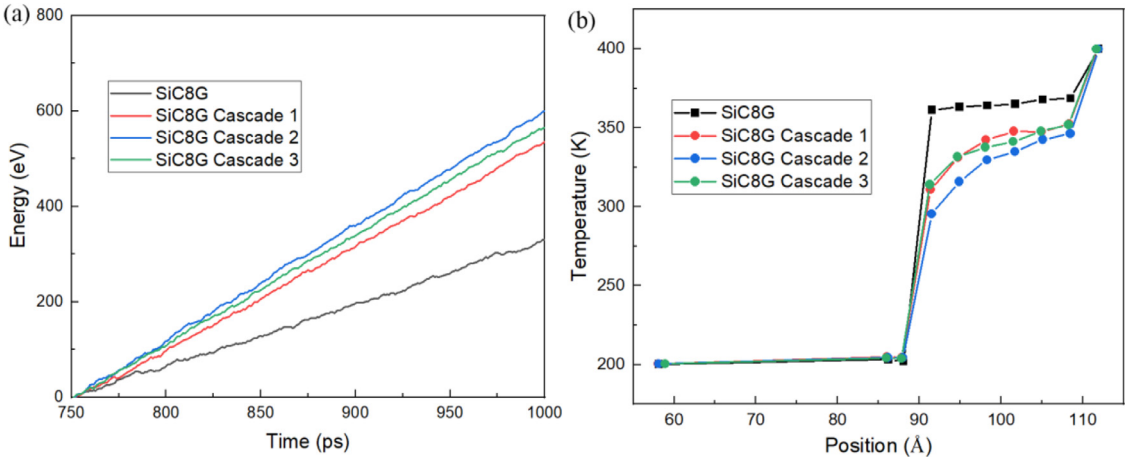

Fig. 9. (a) Cumulative energy change of the heat source/sink and (b) temperature profiles in the NEMD simulations for SiC8G.

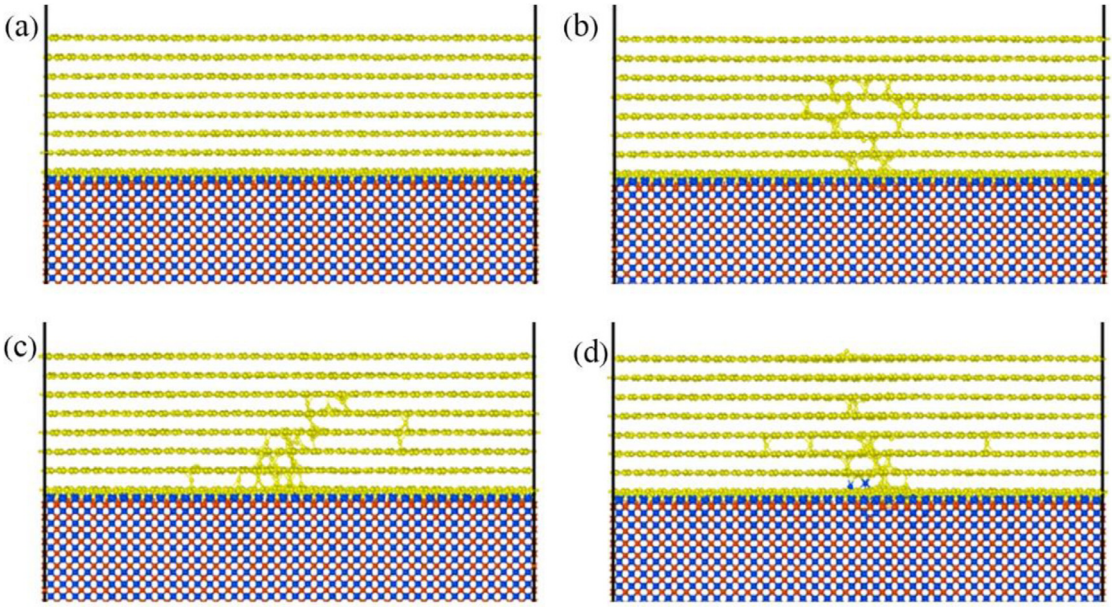

Fig. 10. Interface structures of SiC8G: (a) before irradiation, after (b) cascade 1, (c) cascade 2, and (d) cascade 3. The carbon atoms in graphene layers, silicon, and carbon atoms in SiC are marked in yellow, blue, and pink, respectively.

sides, irradiation can destroy the cubic diamond structure in SiC, which can be identified by the structure identification algorithm [46] implemented in OVITO. Fig. S4 shows the non-perfect cubic diamond atoms of SiC4G and SiC8G before and after cascade 1. More non-perfect cubic diamond atoms occur in SiC4G than that in SiC8G.

The heat fluxes in the unirradiated SiC4G and SiC8G are similar, resulting in the close thermal conductance of 1.30 $\times$ 10^7 and 1.37 $\times$ 10^7 W/(m^2·K), respectively. The reason is the scale effect of heat transfer in nanoscale, where thermal conductivity increases with length, resulting in thermal conductance constant in the ballistic regime and weakly dependent on length in the nanoscale transport regime [35]. Our results are consistent with the conclusion that

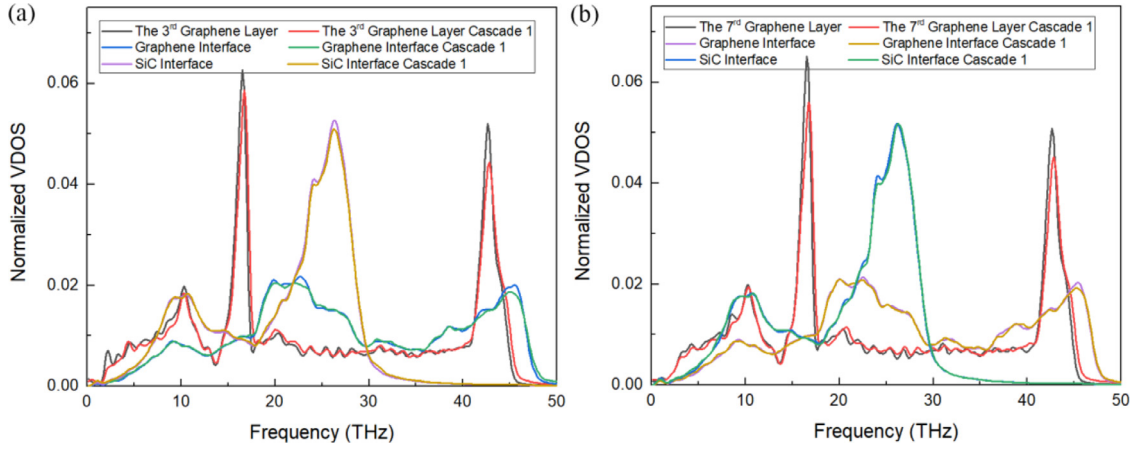

Fig. 11. VDOS comparison of atoms in (a) SiC4G and (b) SiC8G before and after irradiation.

there is no correlation between thermal conductance and graphene layer thickness in graphene/SiO_2 interface [47]. Our simulated thermal conductance on the order of ten's seventh power before irradiation agrees with previous research results [17,48]. After irradiation, the thermal conductance increases by 65.7%, 83.9%, and 75.2% for SiC8G after cascades 1, 2, and 3, respectively, which is comparable with the results of SiC4G. Similarly, the interface thermal resistance is decreased by 59.6%, 68.7%, and 60.3% after cascades 1, 2, and 3, respectively.

The junction area atoms' vibrational properties in SiC4G and SiC8G before and after cascade 1 are analyzed (see Fig. 11). The VDOS of the interface graphene layer is quite different from that of the penultimate graphene layer (the 3rd layer in SiC4G and the 7th layer in SiC8G). Compared to the penultimate graphene layer, the low-frequency peak (around 10 THz) in the VDOS of the interface graphene layer shows great attenuation. The medium frequency peak (around 16 THz) and the high-frequency peak (around 43 THz) shift a bit to the right with attenuation and broadening due to the strong coupling between the interface graphene layer and SiC and the relatively low interaction between graphene layers. Thus, the vibrational modes of the interface graphene layer are greatly affected by SiC. The significant VDOS mismatch between the interface graphene layer and the penultimate layer of graphene is the main reason for the large temperature drop between them (see Figs. 7(b) and 9(b)).

After irradiation, the medium and high-frequency peaks (around 16 and 43 THz) of the penultimate graphene layers reduce in SiC4G and SiC8G due to the defects induced by irradiation. The reason forthermal conductance enhancement after irradiation is that interstitial atoms bond the graphene layers in SiC4L and SiC8L after irradiation (see Figs. 8 and 10). Meanwhile, the temperature of the penultimate graphene layer decreases with the increase of the bonds number between graphene layers (see Figs. 7(b) and 9(b)). Thus, more heat transfers from the first layer to the lower layers of graphene through bonds between graphene layers than that before irradiation, showing increased thermal conductance and decreased interface thermal resistance between SiC and graphene.

4. Conclusions

In summary, the composite structures of 3C-SiC coated with graphene layers are proposed to enhance the irradiation resistance. We investigate the composites' irradiation behavior and thermal conductance performance via MD simulations. The results verify that the graphene layers act as the protective layer of SiC from irradiation with the carbon PKA, with E_d increasing with the graphene layer thickness. The collision cascades with a 1.5 keV carbon PKA show that more graphene layers lead to lower peak and stable vacancy numbers. No clear relationship exists between the incident angle and irradiation resistance. The peak vacancy number increases with temperature, while the survival vacancy number has little correlation with temperature at the range of 300–1200 K. For the heat conduction property study, the largest temperature drop occurs between the interface graphene layer and the penultimate graphene layer instead of the interface layer due to the strongly coupled interface between graphene and SiC. After irradiating with the 1.5 keV carbon PKA, the thermal conductance increases, and the interface thermal resistance decreases because irradiation induces structure change, causing bonds between graphene layers and sp3 carbon atoms formation. Our results provide a practical way to improve the irradiation resistance of materials through coating graphene layers.

Declaration of Competing Interest

The authors declare that they have no known competing financial interests or personal relationships that could have appeared to influence the work reported in this paper.

CRediT authorship contribution statement

Xiaona Huang: Conceptualization, Methodology, Writing – review & editing. **Jiang Guo:** Funding acquisition, Writing – review & editing. **Yanan Yue:** Methodology, Writing – review & editing, Supervision, Funding acquisition.

Acknowledgments

The authors acknowledge the financial support from the National Key Research and Development Program (Nos. 2019YFE0119900 and 2020YFB1709704), Natural Science Foundation of Hubei Province (No. 2021CFB120), National Natural Science Foundation of China (No. 52076156). The authors appreciate the support from the Supercomputing Center of Wuhan University.

Supplementary materials

Supplementary material associated with this article can be found, in the online version, at doi:10.1016/j.ijheatmasstransfer.2022.122988.

References

[1] A.J. Leide, L.W. Hobbs, Z. Wang, D. Chen, L. Shao, J. Li, The role of chemical disorder and structural freedom in radiation-induced amorphization of silicon carbide deduced from electron spectroscopy and ab initio simulations, J. Nucl. Mater. 514 (2019) 299–310.

[2] Z. Tian, X. Chen, X. Xu, Molecular dynamics simulation of the material removal in the scratching of 4H-SiC and 6H-SiC substrates, Int. J. Extrem. Manuf. 2 (4) (2020) 045104.

[3] A.A. Lebedev, Development and investigation of SiC and SiC-based devices, Crystals 10 (12) (2020) 1127.

[4] W. Ma, Y. Liu, S. Yan, T. Miao, S. Shi, Z. Xu, X. Zhang, C. Gao, Chemically doped macroscopic graphene fibers with significantly enhanced thermoelectric properties, Nano Res. 11 (2) (2018) 741–750.

[5] O. Ochedowski, K. Marinov, G. Wilbs, G. Keller, N. Scheuschner, D. Severin, M. Bender, J. Maultzsch, F.J. Tegude, M. Schleberger, Radiation hardness of graphene and MoS_2 field effect devices against swift heavy ion irradiation, J. Appl. Phys. 113 (21) (2013) 214306.

[6] H. Huang, X. Tang, F. Chen, J. Liu, D. Chen, Role of graphene layers on the radiation resistance of copper–graphene nanocomposite: inhibiting the expansion of thermal spike, J. Nucl. Mater. 493 (2017) 322–329.

[7] H. Huang, X. Tang, F. Chen, J. Liu, H. Li, D. Chen, Graphene damage effects on radiation-resistance and configuration of copper–graphene nanocomposite under irradiation: a molecular dynamics study, Sci. Rep. 6 (1) (2016).

[8] Y. Liu, Y. Zeng, Q. Guo, J. Zhang, Z. Li, D.-.B. Xiong, X. Li, D. Zhang, Bulk nanolaminated graphene (reduced graphene oxide)–aluminum composite tolerant of radiation damage, Acta Mater. 196 (2020) 17–29.

[9] S. Kumar, A. Tripathi, S.A. Khan, C. Pannu, D.K. Avasthi, Radiation stability of graphene under extreme conditions, Appl. Phys. Lett. 105 (13) (2014) 133107.

[10] M.X. Navarro, R.R. Delgado, M.G. Lagally, G.L. Kulcinski, J.F. Santarius, Implantation of 30 keV Helium into graphene-coated tungsten, Fusion Sci. Technol. 72 (4) (2017) 713–718.

[11] M.X. Navarro, M. Zamiri, M.E. Griswold, J.F. Santarius, G.L. Kulcinski, M. Lagally, T. Tajima, Outer divertor damage characterization from deuterium plasma bombardment in graphene-coated tungsten in the C-2 W device, Fusion Sci. Technol. 75 (6) (2019) 542–550.

[12] M. Navarro, M. Zamiri, R.B. Jacobson, R. Doerner, J. Santarius, O. Schmitz, M. Lagally, G. Kulcinski, High-quality graphene as a coating for polycrystalline tungsten in low-energy helium and deuterium plasma exposures, J. Nucl. Mater. 552 (2021) 152979.

[13] Q. Wang, C. Wang, Y. Zhang, T. Li, Molecular dynamics study on interfacial thermal conductance of unirradiated and irradiated SiC/C, Nucl. Instrum. Methods Phys. Res. Sect. B 328 (2014) 42–47.

[14] Z. Tian, H. Hu, Y. Sun, A molecular dynamics study of effective thermal conductivity in nanocomposites, Int. J. Heat Mass Transf. 61 (2013) 577–582.

[15] B. Riccardi, P. Fenici, A.F. Rebelo, L. Giancarli, G.Le Marois, E. Philippe, Status of the European R&D activities on SiCf/SiC composites for fusion reactors, Fusion Eng. Des. 51 (2000) 11–22.

[16] R. Wang, S. Xu, Y. Yue, X. Wang, Thermal behavior of materials in laser-assisted extreme manufacturing: Raman-based novel characterization, Int. J. Extrem. Manuf. 2 (3) (2020) 032004.

[17] M. Li, J. Zhang, X. Hu, Y. Yue, Thermal transport across graphene/SiC interface: effects of atomic bond and crystallinity of substrate, Appl. Phys. A 119 (2) (2015) 415–424.

[18] Q.Y. Li, K. Xia, J. Zhang, Y. Zhang, Q. Li, K. Takahashi, X. Zhang, Measurement of specific heat and thermal conductivity of supported and suspended graphene by a comprehensive Raman optothermal method, Nanoscale 9 (30) (2017) 10784–10793.

[19] Q.Y. Li, W.G. Ma, X. Zhang, Laser flash Raman spectroscopy method for characterizing thermal diffusivity of supported 2D nanomaterials, Int. J. Heat Mass Transf. 95 (2016) 956–963.

[20] Q. Wang, N. Gui, X. Huang, X. Yang, J. Tu, S. Jiang, The effect of temperature and cascade collision on thermal conductivity of 3C-SiC: a molecular dynamics study, Int. J. Heat Mass Transf. 180 (2021) 121822.

[21] Y. Li, G. Yue, W.C. Tie, Q.Z. Zhu, T. Yan, Effect of different epoxide and hydroxyl ratios on the heat transport and melting points of graphene/paraffin, Int. J. Heat Mass Transf. 177 (2021) 121533.

[22] T. Ye, H. Yao, Y. Wu, J. Zhang, J. Wu, M. Wang, W. Tian, G.H. Su, S. Qiu, Primary radiation damage characteristics in displacement cascades of FeCrAl alloys, J. Nucl. Mater. 549 (2021) 152909.

[23] P. Chen, A. Chesetti, M.J. Demkowicz, Healing of nanocracks by collision cascades in nickel, J. Nucl. Mater. 555 (2021) 153124.

[24] P. Erhart, K. Albe, Analytical potential for atomistic simulations of silicon, carbon, and silicon carbide, Phys. Rev. B 71 (3) (2005).

[25] Q. Ran, Y. Zhou, Y. Zou, J. Wang, Z. Duan, Z. Sun, B. Fu, S. Gao, Molecular dynamics simulation of displacement cascades in cubic silicon carbide, Nucl. Mater. Energy 27 (2021) 100957.

[26] J.F. Ziegler, J.P. Biersack, in: The stopping and range of ions in matter, Treatise on Heavy-Ion Science, Springer, 1985, pp. 93–129.

[27] S.J. Stuart, A.B. Tutein, J.A. Harrison, A reactive potential for hydrocarbons with intermolecular interactions, J. Chem. Phys. 112 (14) (2000) 6472–6486.

[28] L. Zhang, Z. Shi, Y. Wang, R. Yang, D. Shi, G. Zhang, Catalyst-free growth of nanographene films on various substrates, Nano Res. 4 (3) (2010) 315–321.

[29] Y. Yue, J. Zhang, X. Wang, Micro/nanoscale spatial resolution temperature probing for the interfacial thermal characterization of epitaxial graphene on 4H-SiC, Small 7 (23) (2011) 3324–3333.

[30] H. Guo, X. Yang, Q. Xu, W. Lu, J. Li, H. Dai, H. Ohmori, M. Kosinova, J. Yan, S. Li, T. Goto, R. Tu, S. Zhang, Epitaxial growth and electrical performance of graphene/3C–SiC films by laser CVD, J. Alloy. Compd. 826 (2020) 154198.

[31] X. Song, L. Niu, Effect of uniaxial stress on the threshold displacement energy of silicon carbide, J. Appl. Phys. 124 (10) (2018) 105105.

[32] F. Varchon, R. Feng, J. Hass, X. Li, B.N. Nguyen, C. Naud, P. Mallet, J.-.Y. Veuillen, C. Berger, E.H. Conrad, Electronic structure of epitaxial graphene layers on SiC: effect of the substrate, Phys. Rev. Lett. 99 (12) (2007) 126805.

[33] J. Wallace, D. Chen, J. Wang, L. Shao, Molecular dynamics simulation of damage cascade creation in SiC composites containing SiC/graphite interface, Nucl. Instrum. Methods Phys. Res. Sect. B 307 (2013) 81–85.

[34] T. Schneider, E. Stoll, Molecular-dynamics study of a three-dimensional one–component model for distortive phase transitions, Phys. Rev. B 17 (3) (1978) 1302.

[35] Z. Li, S. Xiong, C. Sievers, Y. Hu, Z. Fan, N. Wei, H. Bao, S. Chen, D. Donadio, T. Ala-Nissila, Influence of thermostatting on nonequilibrium molecular dynamics simulations of heat conduction in solids, J. Chem. Phys. 151 (23) (2019) 234105.

[36] J. Dickey, A. Paskin, Computer simulation of the lattice dynamics of solids, Phys. Rev. 188 (3) (1969) 1407.

[37] T. Liang, P. Zhang, P. Yuan, S. Zhai, D. Yang, A molecular dynamics study on the thermal conductivities of single- and multi-layer two-dimensional borophene, Nano Futur. 3 (1) (2019) 015001.

[38] S. Plimpton, Fast parallel algorithms for short-range molecular dynamics, J. Comput. Phys. 117 (1) (1995) 1–19.

[39] A. Stukowski, Visualization and analysis of atomistic simulation data with OVITO–the Open Visualization Tool, Model. Simul. Mater. Sci. Eng. 18 (1) (2009) 015012.

[40] G. Lucas, L. Pizzagalli, Ab initiomolecular dynamics calculations of threshold displacement energies in silicon carbide, Phys. Rev. B 72 (16) (2005).

[41] L. Malerba, J.M. Perlado, Basic mechanisms of atomic displacement production in cubic silicon carbide: a molecular dynamics study, Phys. Rev. B 65 (4) (2002).

[42] G. Lucas, L. Pizzagalli, Comparison of threshold displacement energies in β-SiC determined by classical potentials and ab initio calculations, Nucl. Instrum. Methods Phys. Res. Sect. B 229 (3–4) (2005) 359–366.

[43] S. Zhao, J. Xue, C. Lan, L. Sun, Y. Wang, S. Yan, Influence of high pressure on the threshold displacement energies in silicon carbide: a Car–Parrinello molecular dynamics approach, Nucl. Instrum. Methods Phys. Res. Sect. B 286 (2012) 119–123.

[44] I. Torrens, M. Robinson, Computer simulation of atomic displacement cascades in solids, in: Interatomic Potentials and Simulation of Lattice Defects, Springer, 1972, pp. 423–436.

[45] M. Hu, D. Poulikakos, Graphene mediated thermal resistance reduction at strongly coupled interfaces, Int. J. Heat Mass Transf. 62 (2013) 205–213.

[46] E. Maras, O. Trushin, A. Stukowski, T. Ala-Nissila, H. Jonsson, Global transition path search for dislocation formation in Ge on Si (001), Comput. Phys. Commun. 205 (2016) 13–21.

[47] K.F. Mak, C.H. Lui, T.F. Heinz, Measurement of the thermal conductance of the graphene/SiO2 interface, Appl. Phys. Lett. 97 (22) (2010) 221904.

[48] R. Mao, B.D. Kong, K.W. Kim, T. Jayasekera, A. Calzolari, M. Buongiorno Nardelli, Phonon engineering in nanostructures: controlling interfacial thermal resistance in multilayer-graphene/dielectric heterojunctions, Appl. Phys. Lett. 101 (11) (2012) 113111.